PMAS
Proceedings of the Mongolian Academy of Sciences
Vol. 65 No 01(253) 2025
DOI: https://doi.org/10.5564/pmas.v65i01.4204

ARTICLE

Water accounting: A case study in the Buir Lake - Khalkh River Basin

Purevsuren Munkhtur*, Batnyam Tseveengerel and Bayanjargal Bumtsend

Division of Physical Geography, Institute of Geography and Geoecology, Mongolian Academy of Sciences, Ulaanbaatar, Mongolia

ARTICLE INFO: Received: 24 Sep, 2024; Accepted: 28 Mar, 2025

Abstract: Arid and semi-arid regions face increasing shortage of water resources due to climate variability and competing land and water uses, yet reliable information on water availability and consumption remains limited. This study addresses the critical gap in understanding water dynamics in such environments by analyzing the Buir Lake–Khalkh River Basin in Mongolia using the Water Accounting Plus (WA+) framework. The research aims to quantify water balance components and identify how land use and land cover types influenced water availability between 2010 and 2021. Climatic datasets from WorldClim, SSEBop, and GRACE-FO were employed to estimate precipitation (P), evapotranspiration (ET), and water yield (WY). Esimates showed an average annual precipitation of 298.5 mm, with notable peaks of 386.3 mm in 2013 and minimal below 250 mm during dry years. Similarly, ET demonstrates considerable variability, averaging 274.9 mm/year; maximum value was observed in 2013 at 434.8 mm, whereas the lowest value, recorded in 2017, was 200.4 mm. The average annual water yield for the basin is quantified at 23.8 mm, with specific land cover types, such as the steppe, yielding positive values (64.1 mm), while water bodies exhibited a significant deficit of -342 mm. Furthermore, WA+ resource and evapotranspiration sheets were generated for the years 2018 and 2019. In 2018, net inflow was calculated at 8.1 km³/year, of which 4.6 km³/year was attributable to landscape evapotranspiration, resulting in 3.5 km³/year deemed exploitable. In contrast, 2019 recorded a lower inflow of 7.5 km³/year, with 5.4 km³/year lost to ET. This research elucidates the interactions among precipitation, ET, and WY, emphasizing the critical influence of land management classes on water consumption patterns. Additionally, the findings contribute to the formulation of sustainable water management strategies in arid regions and provide a methodological framework for evaluating water resources in similarly stressed basins through the integration of remote sensing and water accounting methodologies.

Keywords: *Water balance components, Semi-Arid basin hydrology, Land use impact on hydrology;*

INTRODUCTION

Water is a critical resource integral to the functioning of ecosystems, agricultural productivity, and human health [1] in Mongolia. In regions, such as Mongolia, where water resources are both scarce and unevenly distributed, effective management is imperative for achieving sustainable use and equitable access [2], [3]. However, arid and semi-arid regions of Mongolia are experiencing increasing stress in water resources mostly due to the combined effects of climate variability,

***Corresponding author, email**: purevsurenm@mas.ac.mn https://orcid.org/0000-0003-4994-1744

Vol. 65 No 01(253) 2025
DOI: https://doi.org/10.5564/pmas.v65i01.4204

population growth [4], and expanding land and water use activities for exploitation and livestock husbandry [5]. Despite this, reliable and spatially explicit information on water availability and consumption remains limited, particularly at the basin scale [6], [7]. This lack of data and understanding presents a significant barrier to the formulation of sustainable water management strategies and hampers informed decision-making.

The application of water accounting methods to assess water provisioning services can provide valuable insights into regional water dynamics, revealing areas of stress and inefficiency [8]. Nonetheless, challenges, such as data gaps and variability in water-use reporting continue to pose significant obstacles [9]. Water accounting, particularly through frameworks like Water Accounting Plus (WA+), offers a comprehensive methodology for quantifying and managing water resources[10]. The original concept of water accounting, as introduced by Molden (1997), focused on analyzing irrigation systems using observed data, and later evolved to incorporate remote sensing data to provide spatially aggregated performance metrics for these systems [11]. The WA+ framework has since developed to integrate hydrological processes with land use and manage water flows in relation to ecosystem services within river basins [12]. This enhanced approach enables detailed assessments by synthesizing diverse data sources, thereby facilitating a nuanced understanding of water yield and availability [13], [14], [15]. It is particularly effective for evaluating water provisioning services, which encompass the capacity of water systems to supply fresh water for a range of uses [8].

This study is focused on the Buir Lake-Khalkh River Basin, a significant hydrological region in Mongolia that faces challenges due to its arid climate and increasing water demands [16]. The research aims to accomplish three specific objectives: (1) estimating the components of water balance to elucidate the distribution and availability of water resources, (2) calculating water yield for dominant land use/land cover (LULC) types from 2010 to 2021 to assess the impact of different land types on water yield, and (3) generating WA+ outcomes, including resource base and evapotranspiration sheets, to provide detailed insights into water resource dynamics and provisioning. By utilizing the WA+ framework, this study seeks to address existing information gaps and support the development of more effective and sustainable water management strategies in the basin.

Study area

The Buir Lake–Khalkh River Basin, located in Eastern Mongolia, spans latitudes N46.51° to N47.99° and longitudes E116.99° to E119.93°, covering 23,755.8 km² [6]. Elevations range from 547 to 1,490 meters above sea level (Figure 1). This region represents the Central Asian stipa-steppe zone [17]. Eastern Mongolia has an extreme continental climate but generally warm due to the geographical location and topographic features. According to the Koppen-Gieger climate classification system, most of the study area is classified as Dwb (monsoon-influenced warm-summer humid continental climate) and Dwc (monsoon-influenced subarctic climate) due to the influence of the East Asian Winter Monsoon since the middle Holocene [18]. Furthermore, the climatic regionalization map of Mongolia developed by Tsegmid and Vorovev (1990), identifies three distinct climatic zones within the study area: semi-arid and cool, arid and cool, and moderately humid with moderately cold conditions [19]. The average annual air temperature is +0.5°C and the annual precipitation is around 413.5 mm, mostly associated with the summer monsoon of May to September (average of 356.8 mm falls) based on the measured values of the Khalkh Gol meteorological station for the years 1993-2022 [20].

Vol. 65 No 01(253) 2025
DOI: https://doi.org/10.5564/pmas.v65i01.4204

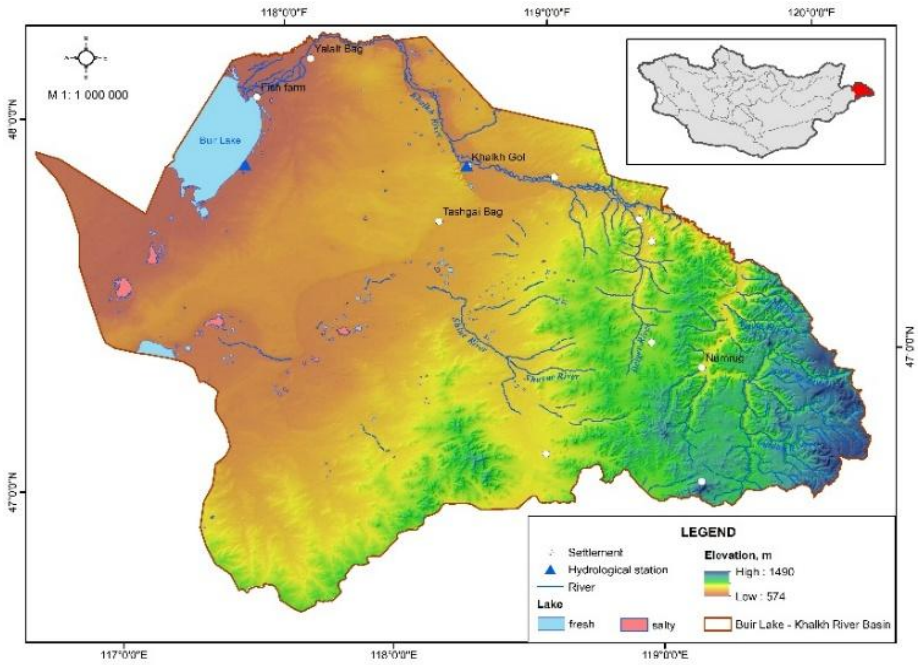

Figure 1. Study area map.

The basin's surface water resource totals approximately 1,023 m³/year [6]. The main tributary, the Khalkh River, originates in the Greater Khingan Mountains and splits into two branches: the Khalkh River flowing into Buir Lake and the Sharilijiin River, which flows into the Orshuun River, the lake's sole outlet [6]. The Khalkh River's catchment area is 78,360 km², with 7,440 km² in Mongolia, and it extends 435 km in total length, 264 km within Mongolia [21]. The biggest natural water reservoir in the study area is the Buir Lake, the largest freshwater lake in Eastern Mongolia bordering with China. The Buir Lake also includes a large portion of wetlands important for breeding and resting ground for many species of migratory birds, as it is lies along the East Asian-Australasian Flyway [22]. In 2014, Lake Buir was listed as an annex to the Ramsar Convention on Wetlands of International Importance, especially in the habitat of waterfowl. The Lake 40 km long from the northeast to the southwest, its width is 21 km, it has a coastline, which is 118 km long, a catchment area of 20,200 km^2 and an area of 615 km^2[23].

Other main rivers in the basin are Guut, Numrug, Nariin and Khaliut.

MATERIALS AND METHODS

Water accounting plus (WA+) approach

The Water Accounting Plus (WA+) framework was developed to provide explicit spatial information on net water withdrawal and depletion processes in complex river basins [12]. Initially introduced by Molden [11] in 1998, the framework was further refined by Karimi [12], [24] to incorporate a comprehensive analysis of all water-use sectors within river basins. The core principles of the WA+ framework are based on the mass water balance approach [12]. This approach establishes a direct relationship between the outflows from a given area and net inflow and depletion, primarily through quantifiable evapotranspiration (ET) processes [12]. A key advantage of this method is that it eliminates the need for direct measurements of withdrawals and return flows, as depletion can be estimated using satellite-based measurements. Theoretically, the total water balance in a basin over a specific period can be expressed by the following equation:

Vol. 65 No 01(253) 2025
DOI: https://doi.org/10.5564/pmas.v65i01.4204

$$P + \left(Q_{in}^{SW} + Q_{in}^{GW}\right) - ET - \left(Q_{out}^{SW} + Q_{out}^{GW}\right) + \Delta S = 0 \qquad \text{(Eq 1)}$$

Where, P represents precipitation, $\left(Q_{in}^{SW} + Q_{in}^{GW}\right)$ denote surface and groundwater inflows, ET refers to total evapotranspiration, $(Q_{out}^{SW} + Q_{out}^{GW})$ represents surface and groundwater outflows, and ΔS signifies the change in storage. However, within a single unit of the managed water-use sector, where water withdrawals occur, the water balance equation can be expressed as follows:

$$P + (Q_{w}^{SW} + Q_{w}^{GW}) - (ET_{prec} + ET_{Q}) - (Q_{R}^{SW} + Q_{R}^{GW}) = 0 \qquad \text{(Eq 2)}$$

In this equation, $(Q_{w}^{SW} + Q_{w}^{GW})$ represents withdrawals from surface water and groundwater, ET_{prec} denotes evapotranspiration from precipitation, ET_{Q} refers to the incremental evapotranspiration, and $(Q_{R}^{SW} + Q_{R}^{GW})$ signifies the return flow to surface water and groundwater.

Estimation of total evapotranspiration (ET) is often challenging due to the need for sophisticated models, high-quality data, and attention to spatial and temporal variations.

The mass water balance approach simplifies this by distinguishing ET from precipitation and incremental ET, allowing for easier tracking of water depletion across different areas and land use classes [12]. In WA+ framework, the ET from precipitation (ET_{prec}) is termed green ET (ET_{green}), while the incremental ET (ET_{Q}) is called blue ET (ET_{blue}). Water depletion, defined as actual evapotranspiration (ET_{actual}), is further divided into ET_{green} and ET_{blue} as described in Figure 2.

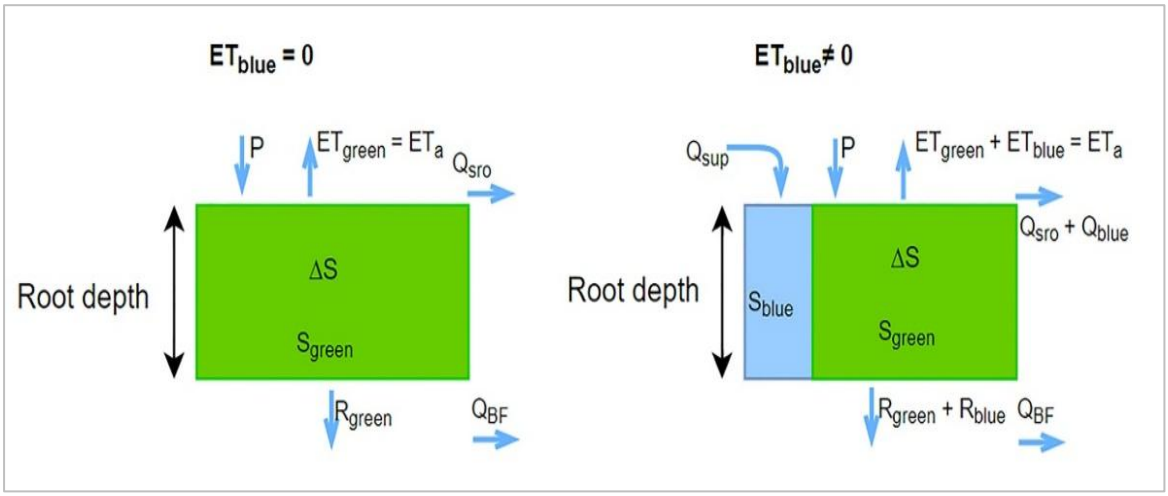

Figure 2. Main schematization of the WA+ framework

When precipitation reaches land, it takes either green or blue water pathways [25]. Green water is stored in the unsaturated soil layer, where soil evaporation occurs. Furthermore, soil evaporation (E) occurs when water in the unsaturated zone of soil moves upward through capillary action and evaporates at the surface [26]. Thus, in this study, we considered evaporation from unsaturated soil as a ET_{green}. The water that is stored in the rivers, streams, surface-water bodies, and groundwater forms the blue water resources, and ET_{blue} is estimated by subtracting ET_{green} from ET_{actual}.

Input data pre-processing

The key data required for water accounting assessment were sourced from multiple datasets, as detailed in Table 1.

Vol. 65 No 01(253) 2025
DOI: https://doi.org/10.5564/pmas.v65i01.4204

Climatic data, including precipitation and evapotranspiration, were obtained from WorldClim and the SSEBop product. WorldClim, a high-resolution global climate database, is downscaled from CRU-TS-4.06 by the Climatic Research Unit at the University of East Anglia [27]. For this study, monthly and yearly precipitation data from WorldClim 2.1 were collected for the years 2010–2020 and resampled to 0.001° for analysis in ArcMap 10.8.2. Given uncertainties in satellite-based precipitation data, monthly precipitation measurements (2013–2021) from the Khalkh Gol meteorological station (sourced from: National Agency Meteorology and the Environmental Monitoring) were used to validate WorldClim data accuracy. Evapotranspiration data from the SSEBop product cover the years 2010–2020 and are based on the Simplified Surface Energy Balance approach, integrating ET fractions from MODIS thermal imagery and reference ET using a thermal index method [28], [29].

Table 1. An overview of used input data.

№	Input data	Data source	Resolution	
			Temporal	Spatial
A.	***Satellite products***			
1	Precipitation (P)	WorldClim	Monthly (2010-2022)	0.041666667°
2	Evapotranspiration (ET)	SSEBop		0.009652°
3	Water storage change	GRACE-FO		Point value
4	Land use and land cover (LULC)	Landsat-SVM	2022	30 m
5	Transpiration (T)	WaPOR V3	Yearly (2018-2022)	300 m
6	Evaporation (E)	WaPOR V3		
7	Interception (I)	WaPOR V3		
8	Actual evapotranspiration and interception (AETI)	WaPOR V3		
B.	***Measured data***			
9	Precipitation ($P_{measured}$)	NAMEM	Monthly (2013-2021)	*

Land use and land cover data were classified using the Support Vector Machine (SVM) method with ENVI and ArcMap 10.8.2 software, based on Landsat imagery with a 30-meter spatial resolution. SVM, a non-parametric machine learning technique, identifies key spectral features with fewer training samples compared to other methods, leading to accurate land cover classification [30]. Landsat images for classification were acquired during the summer of 2022 via the OLI sensor from the USGS Earth Explorer website, as detailed in Table 2.

Table 2. Selected Landsat images and description.

№	Satellite	Sensor	Data of registration	Path/Row	Resolution, m
1	Landsat 8	OLI	31/07/2022	124/27	30
2	Landsat 8	OLI	31/07/2022	124/28	30
3	Landsat 9	OLI-2	01/08/2022	123/27	30

Land cover refers to the physical characteristics of vegetation (e.g., grass, savannah, forest), while land use pertains to the purpose of that land cover (e.g., pasture, crop farming, soccer field) [31]. Therefore, we classified six land cover types: forest, meadow steppe, forest steppe, steppe, sandy plains, and water bodies. Additionally, we

Vol. 65 No 01(253) 2025
DOI: https://doi.org/10.5564/pmas.v65i01.4204

identified five land use classes: settlement, road, tourism, agriculture, and mining. For application within the WA+ framework, as outlined by Karimi et al, 2013 [12] and converted by Singh et al, 2022 [15], all LULC types were categorized into four main management classes: protected land use (PLU), utilized land use (ULU), modified land use (MLU), and managed water use (MWU) as stated in Table 3.

Table 3. Description of four main land use management classes of WA+ framework.

№	Type	Description
1	Protected Land Use (PLU)	Areas that have a special nature status and are protected by the National Governments or International NGO's
2	Utilized Land Use (ULU)	Areas that have a light utilization with a minimum anthropogenic influence, where the water flow is essentially natural
3	Modified Land Use (MLU)	Areas where the land use has been modified. Water is not diverted but land use affects all unsaturated zone physical process such as infiltration, storage, percolation and water uptake by roots; this affects the vertical soil water balance
4	Managed Water Use (MWU)	Areas where water flows are regulated by humans via irrigation canals, pumps, hydraulic structures, utilities, drainage systems, ponds etc.

In addition, total water storage changes (TWSA) within the study area were analyzed using data from the Gravity Recovery and Climate Experiment (GRACE) and its successor mission, GRACE Follow-On (GRACE-FO), covering the period from January 2010 to December 2021. Monthly Level-3 mascon solutions with a spatial resolution of approximately 1° were retrieved from the NASA GRACE-FO archive[32]. Anomalies were derived and subsequently processed to minimize correlated noise and leakage errors through the application of a 300 km Gaussian smoothing filter. The resulting smoothed TWSA fields were then spatially constrained using a basin mask, enabling the calculation of area-weighted monthly anomalies. Additionally, transpiration (T), evaporation (E), and interception (I) data were sourced from Water Productivity through Open access of remotely sensed data (WAPOR V3) dataset by the Food and Agriculture Organization (FAO), which offers comprehensive global metrics on water productivity and related parameters.

RESULTS AND DISCUSSION

In this section, the results of the water balance and WA+ framework will be presented through several sub-results. The spatiotemporal distribution of precipitation and the variability of evapotranspiration across the study area will be described, with changes in water storage relative to long-term averages highlighted. The interrelation among key water balance components - precipitation (P), evapotranspiration (ET), and Total Water Storage Anomaly (TWSA) - will be examined, including the estimation of water yield (WY) for the study years. The variation in water yield across different land use/land cover (LULC) types will also be explained. Finally, the outcomes from the WA+ Resource Base and Evaporation Sheets will be detailed, offering a comprehensive overview of water resources, inflows, outflows, and evaporation patterns.

Spatiotemporal distribution of precipitation

The left bar chart in Figure 3 displays annual precipitation totals from 2010 to 2021. The long-term mean annual precipitation is 298.5 mm, with a significant variation observed over the study period. Precipitation increased from 2010 to 2013, peaking at 386.3 mm in 2013, followed by a decline in 2014 and 2015, with totals dropping below 260 mm. From 2016 to 2019, precipitation levels varied moderately between 228.9 and 320.8 mm. A notable resurgence in 2021 nearly approached the peak levels recorded in 2013.

Vol. 65 No 01(253) 2025
DOI: https://doi.org/10.5564/pmas.v65i01.4204

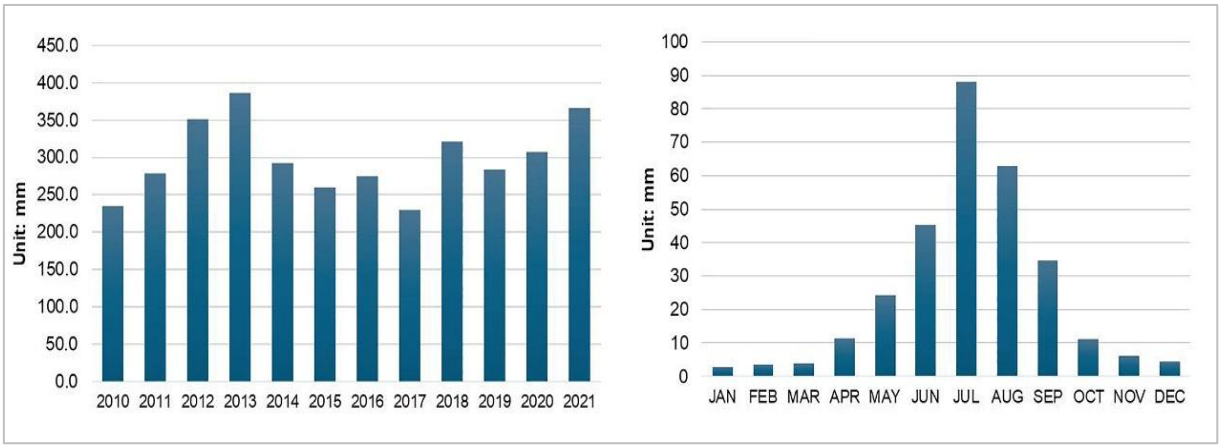

Figure 3. Changes in mean annual and monthly precipitation.

The right bar chart in Figure 3 illustrates the monthly distribution of precipitation, highlighting the region's strong seasonal pattern. The data shows that most precipitation occurs between May and September, with July receiving the highest amount at nearly 90 mm. This pronounced seasonality is characteristic of monsoon-influenced climates, where the majority of annual precipitation is concentrated over a brief period.

The scatter plot in (Figure 4) compares observed precipitation values from NAMEM at the Khalkh Gol meteorological station (2013-2021) with WorldClim-predicted values. Statistical metrics were used to assess the model's performance. The determinant coefficient of 0.70 indicates that 70% of the variance in observed precipitation can be explained by WorldClim predictions, reflecting a relatively strong relationship. The Pearson correlation coefficient of 0.83 further confirms a strong positive linear correlation. The Root Mean Square Error (RMSE) of 17.4 mm quantifies the average deviation of the predicted values from the observed, highlighting a degree of prediction error.

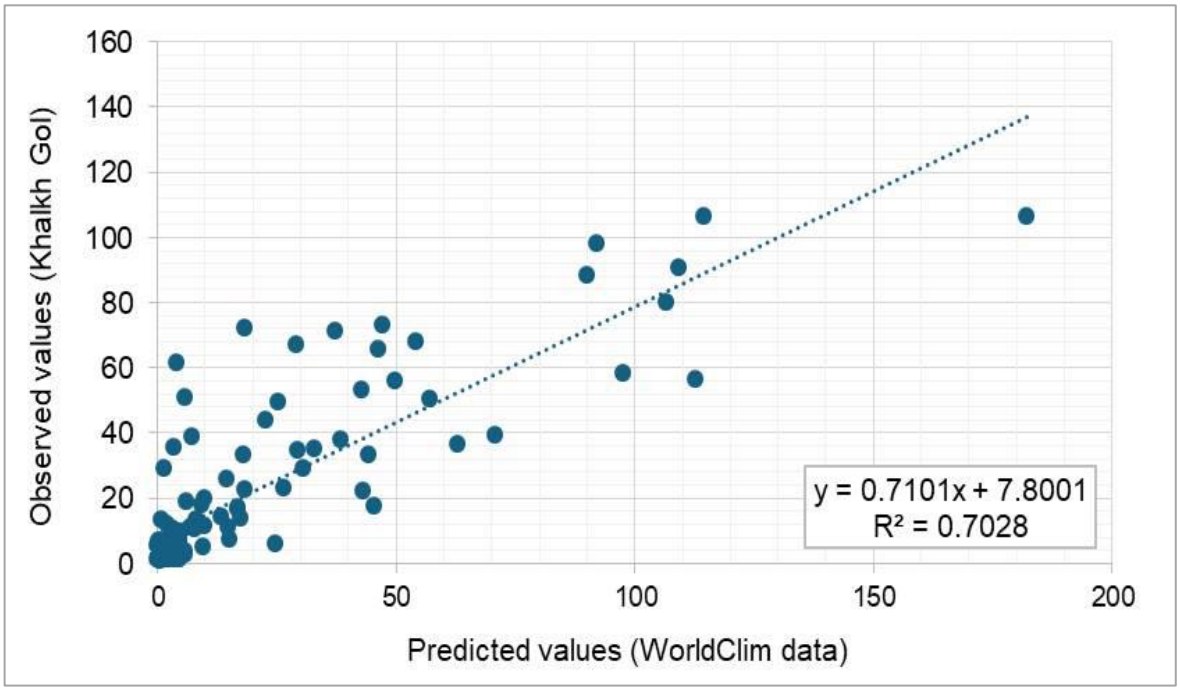

Figure 4. Comparison of Observed vs. Predicted Precipitation.

Vol. 65 No 01(253) 2025
DOI: https://doi.org/10.5564/pmas.v65i01.4204

Figure 5 presents maps illustrating the spatial distribution of annual precipitation for a dry year (2017), a wet year (2013), and the long-term mean in the Khalkh River – Buir Lake Basin according to the WorldClim data. The mean annual precipitation ranged from 228.9 mm in 2017 to 386.3 mm in 2013. The first map depicts the precipitation distribution for 2017, characterized as a dry year, with a color gradient from deep orange to yellow, indicating low precipitation levels, mostly between 175 mm and 339 mm annually. In contrast, the 2013 map shows a shift to green and blue hues, especially in the eastern and northern regions, where precipitation levels reaching up to 597 mm (maximum) annually.

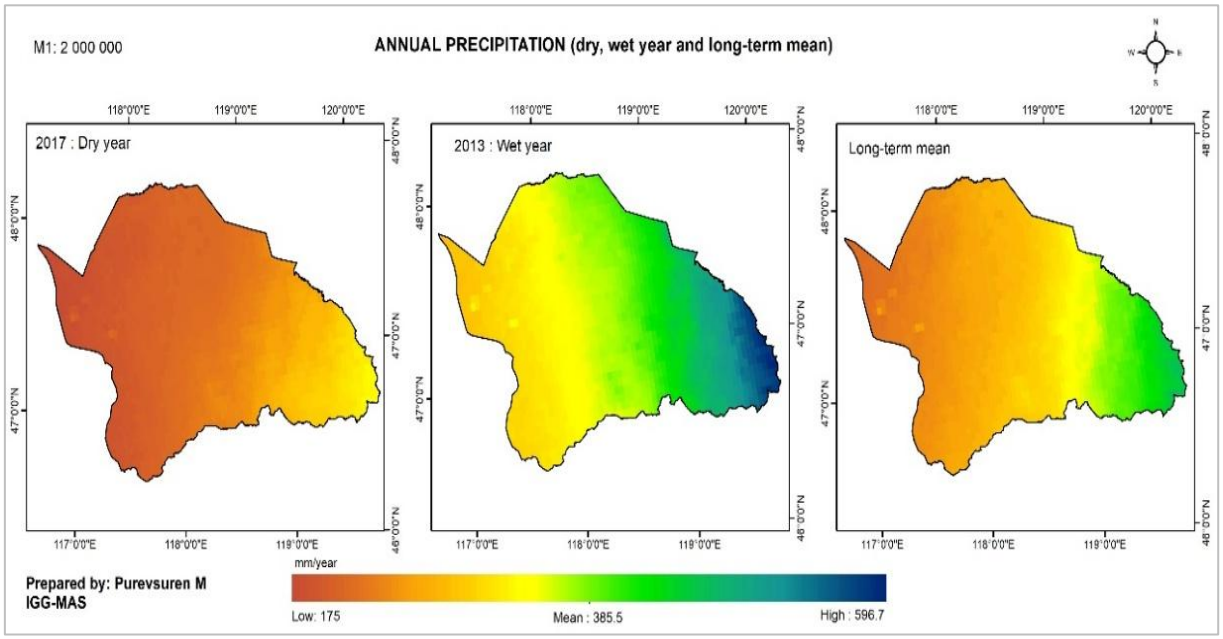

Figure 5. Mean annual precipitation and corresponding dry and wet years.

Spatiotemporal variability of evapotranspiration

In this study, the seasonal and inter-annual variability of evapotranspiration (ET) in the basin was analyzed using SSEBop ET dataset. The long-term mean annual ET is 274.9 mm (2010-2021), with temporal variability depicted in Figure 6.

The left bar chart in Figure 6 displays annual ET data from 2010 to 2021, highlighting significant fluctuations over the years. The highest ET value of 434.8 mm was recorded in 2013, followed by a decline, with the lowest value of 200.4 mm in 2017. From 2018 onwards, ET values gradually increased but did not return to the 2013 peak. The right bar chart in Figure 6 shows the monthly distribution of ET, revealing a clear seasonal pattern with significant increases during warmer months, peaking in June and July at nearly 65 mm. This indicates a strong seasonal component, with the highest ET values occurring in spring and early summer.

Vol. 65 No 01(253) 2025
DOI: https://doi.org/10.5564/pmas.v65i01.4204

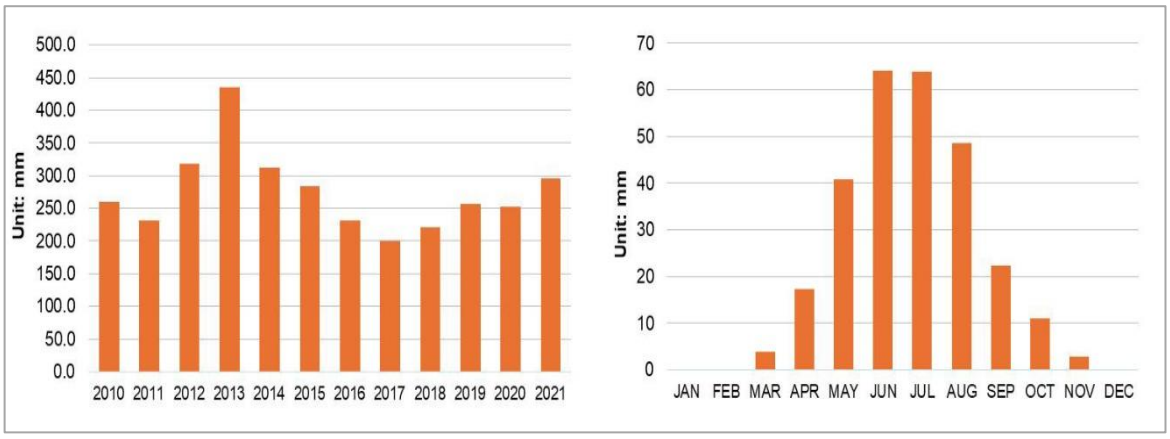

Figure 6. Changes in mean annual and monthly actual evapotranspiration.

Figure 7 presents maps depicting the spatial distribution of actual evapotranspiration (ET) for a dry year (2017), a wet year (2013), and the long-term mean. The 2017 map is blue and light blue, indicating lower ET rates across most of the area, with higher ET values in the northwest, suggesting localized moisture retention, particularly around Buir Lake. In contrast, the 2013 map displays increased ET due to higher rainfall or more favorable climatic conditions, reflected in a broader range of colors indicating greater water availability and elevated evapotranspiration.

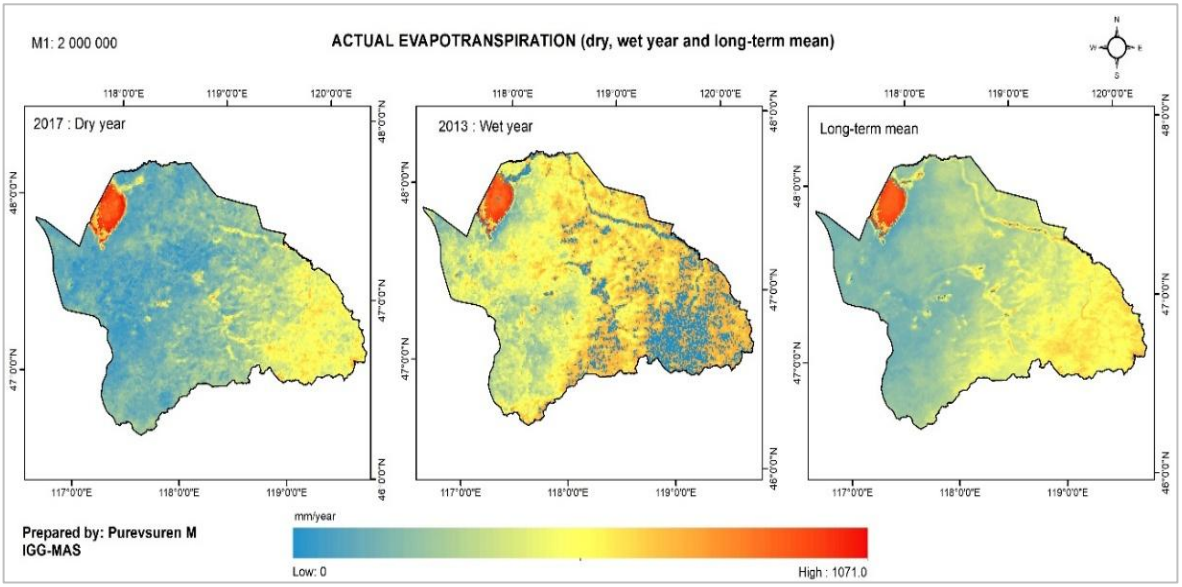

Figure 7. Mean annual actual evapotranspiration and corresponding dry and wet years.

Changes in total water storage

Figure 8 illustrates the total water storage change from 2010 to 2021, based on GRACE-FO data from the Jet Propulsion Laboratory (JPL) and the Center for Space Research (CSR). The graph reveals an overall increase in TWSA over the study period, indicating a net gain in water storage. Both JPL and CSR datasets show similar trends, with some variations in magnitude and timing. From 2010 to 2012, both datasets indicate stability with minor fluctuation. A noticeable increase in TWSA begins around 2013, especially in the CSR dataset, which shows several peaks above 100 mm, reflecting wetter conditions or enhanced water storage.

After 2015, TWSA gradually declines, returning to near baseline levels by 2017, suggesting reduced water storage

Vol. 65 No 01(253) 2025
DOI: https://doi.org/10.5564/pmas.v65i01.4204

due to drier conditions or increased water use. From 2018 to 2021, TWSA increases noticeably, with a sharp rise in the CSR dataset around 2020, reaching 200 mm. The JPL dataset also indicates an upward trend, although less pronounced. The overall increase in TWSA, particularly the sharp rise in recent years, suggests potential periods of water surplus that may have significant implications for water resource management and utilization.

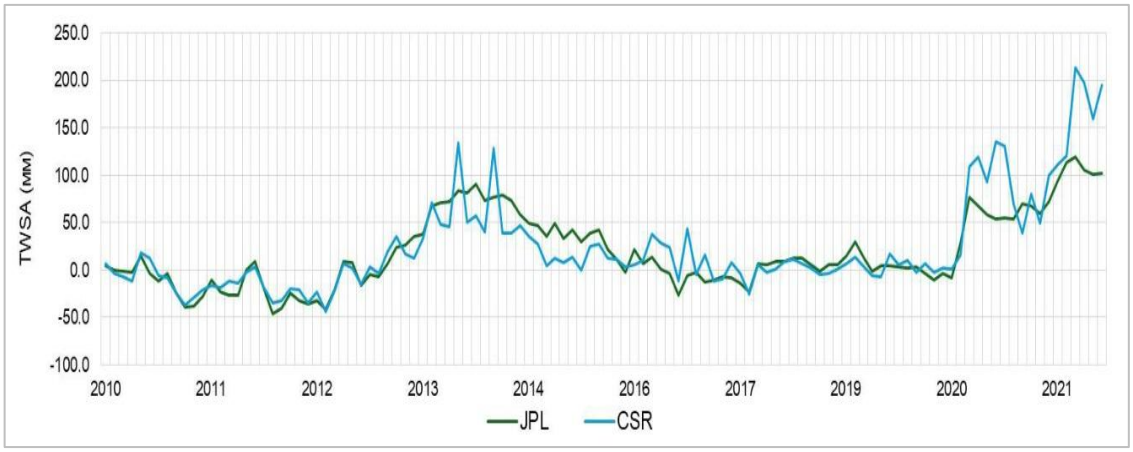

Figure 8. Spread of the TWSA estimated from the different GRACE solutions.

Interrelation of water balance components

Water balance of a region is governed by the interplay between precipitation (P), actual evapotranspiration (ET), and total water storage change (ΔS). These factors are interconnected and they collectively determine the availability and distribution of water within a lake and river system. From 2010 to 2021, precipitation (P) and evapotranspiration (ET) showed notable fluctuations. Peaks in P and ET occurred in 2012 and 2013, indicating high water availability. From 2014 to 2017, P decreased to around 200 mm, while ET remained stable at about 250 mm, creating a water deficit. This imbalance led to a significant decline in total water storage anomaly (TWSA) during these years, with a notable negative anomaly between 2015 and 2017, suggesting drought conditions. Post-2017, TWSA began to recover as P increased slightly and ET stabilized.

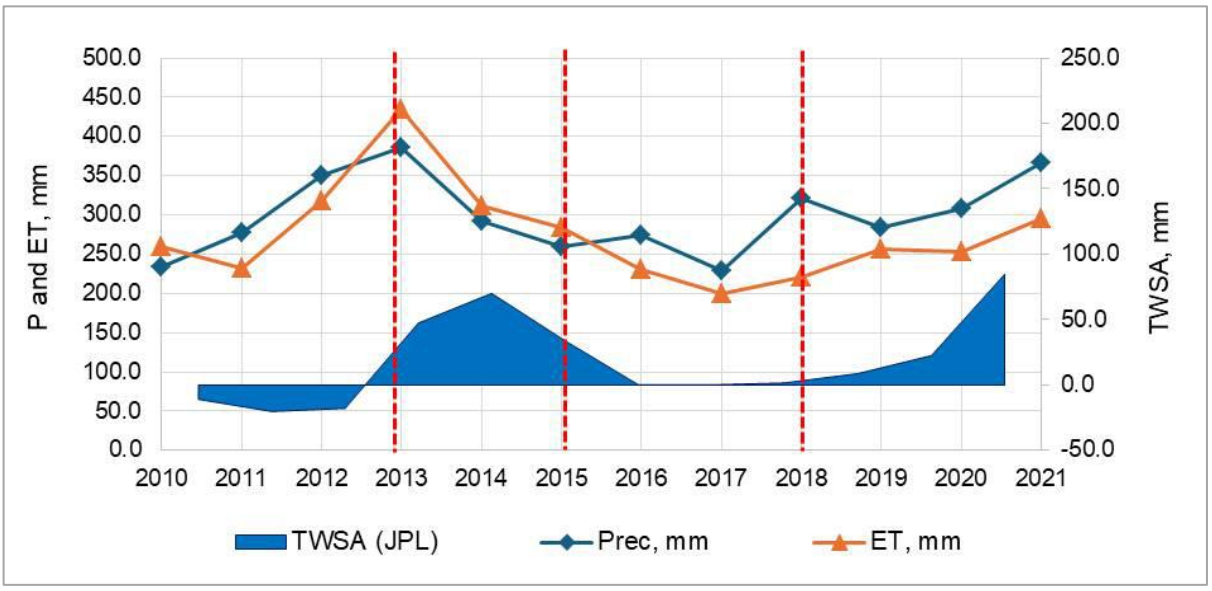

Figure 9. Basic water balance of Buir Lake – Khalkh River Basin based on remote sensing data.

Vol. 65 No 01(253) 2025
DOI: https://doi.org/10.5564/pmas.v65i01.4204

The red vertical dashed lines in Figure 9 marked four transition periods, indicative of shifts in water balance dynamics. During the first period (2010–2012), precipitation and actual evapotranspiration (ET) were relatively balanced, and total water storage anomaly (TWSA) exhibited only minor fluctuations, suggesting stable hydrological conditions. In the second period (2013–2015), ET exceeded precipitation, yet TWSA remained relatively high, particularly in 2013. This apparent contradiction can be attributed to the exceptionally high precipitation recorded in 2013 (386.3 mm), which, despite being offset by elevated ET (434.8 mm), contributed to temporary positive water balance. The resulting increase in soil moisture, surface water, and possibly groundwater storage was captured by GRACE-derived TWSA and buffered the system against immediate losses.

In 2014–2015, precipitation declined significantly while ET remained high, likely sustained by residual moisture and storage from the previous wet year. This lag in hydrological response reflects the capacity of basin systems to store and gradually release water, highlighting the importance of antecedent conditions in modulating short-term water balance indicators. During the third period (2016–2018), precipitation and ET values converged, leading to a stable TWSA near zero and indicating hydrological equilibrium. Finally, from 2019 to 2021, increasing precipitation alongside steady ET supported the recovery of TWSA, suggesting enhanced water availability and system recharge.

Mapping of Water Yield (excluding TWSA)

Water yield, the difference between precipitation and evapotranspiration, indicates water availability in the Buir Lake-Khalkh River Basin. The basin's average annual water yield is 23.8 mm/year for the study period. Negative water yields occurred in 2010, 2013, 2014, and 2015, corresponding with years where ET exceeded precipitation. Among these, 2013 experienced the lowest water yield (-48.6 mm), which is visibly corroborated in the map by the dominance of grey to red areas, particularly in the northwestern region, indicating widespread water-deficit zones. The years 2014 and 2015 show similar spatial patterns, with the central and northern portions of the watershed largely exhibiting non-generating or negative yield areas. Positive water yields were observed for the majority of the study period, particularly pronounced in 2018 and 2021.

In 2018, which had the highest WY value (100 mm), the map illustrates an extensive spread of blue areas across the watershed, reflecting strong water generation, especially in the southern and central zones. Conversely, 2019 recorded the lowest positive WY (26.2 mm), with less pronounced blue zones, suggesting more moderate water yield and slightly elevated ET compared to precipitation. Consequently, we selected those two years 2018 (highest in WY), and 2019 (lowest in WY) as a representative years for establishing WA+ resource and evapotranspiration sheet in the next sub-sections.

Vol. 65 No 01(253) 2025
DOI: https://doi.org/10.5564/pmas.v65i01.4204

Water yield for different LULC types

The LULC map from SVM classification (Figure 11) shows a predominance of natural landscapes in the study area. The steppe and forest steppe are the largest land cover types, with steppe grassland providing crucial biodiversity support, livestock grazing, and ecological balance. Forest steppe, a mix of grassland and forest, aids in carbon sequestration and biodiversity maintenance. Sandy plains, covering 8.8%, are found around riverbeds in the central area and near Buir Lake in the northwest.

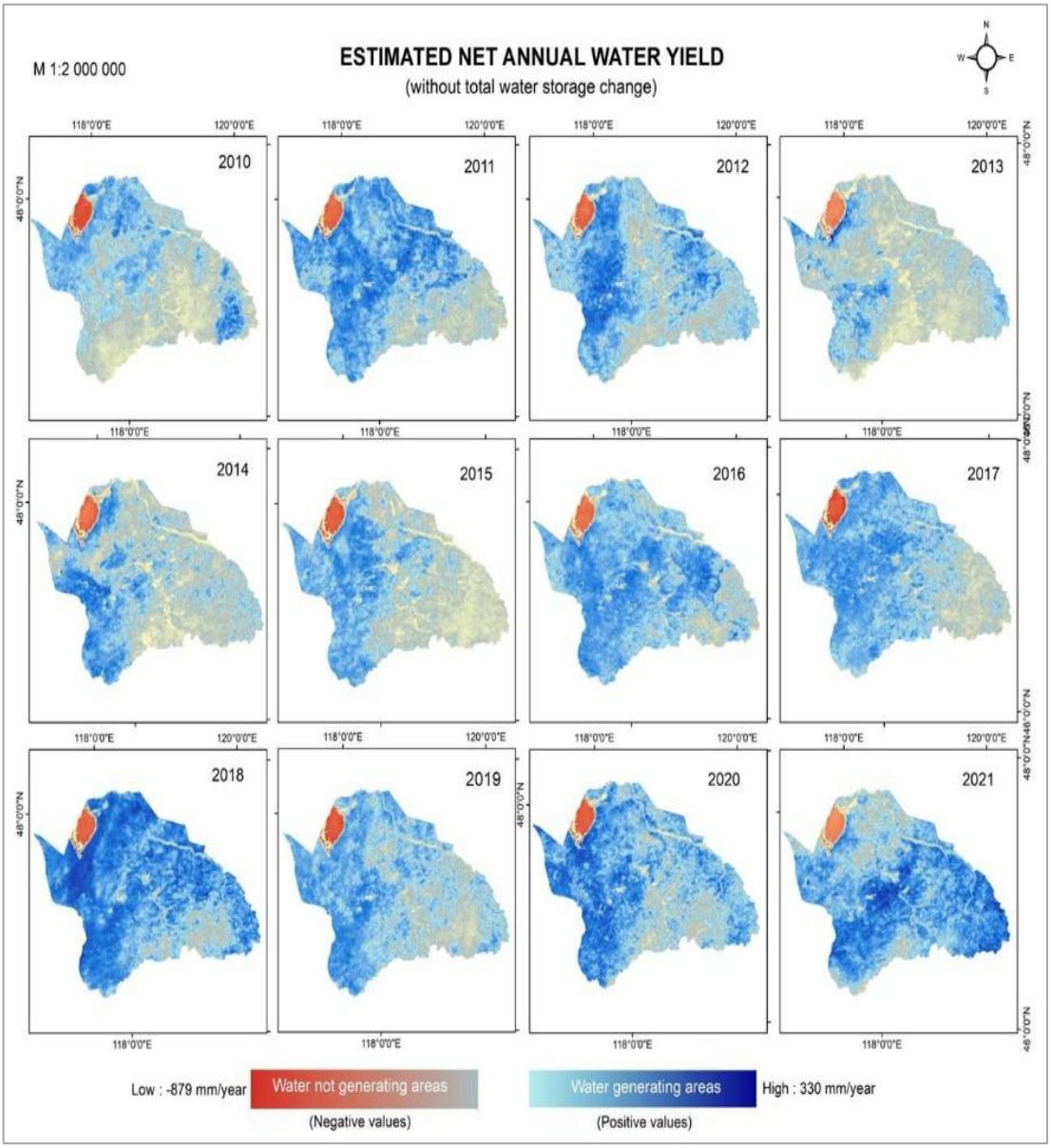

Figure 10. Water Yield, by mm/year.

Meadow steppe constitutes 7.8% of the basin, while forests in the southern and southeastern regions make up 5.2%. Water bodies, including Buir Lake and nearby rivers, account for 4.5% of the area, highlighting the importance of water resources. Human impact is minimal, with agricultural areas at 2.2% and roads at 0.3%, indicating the basin remains largely undeveloped and natural.

Vol. 65 No 01(253) 2025
DOI: https://doi.org/10.5564/pmas.v65i01.4204

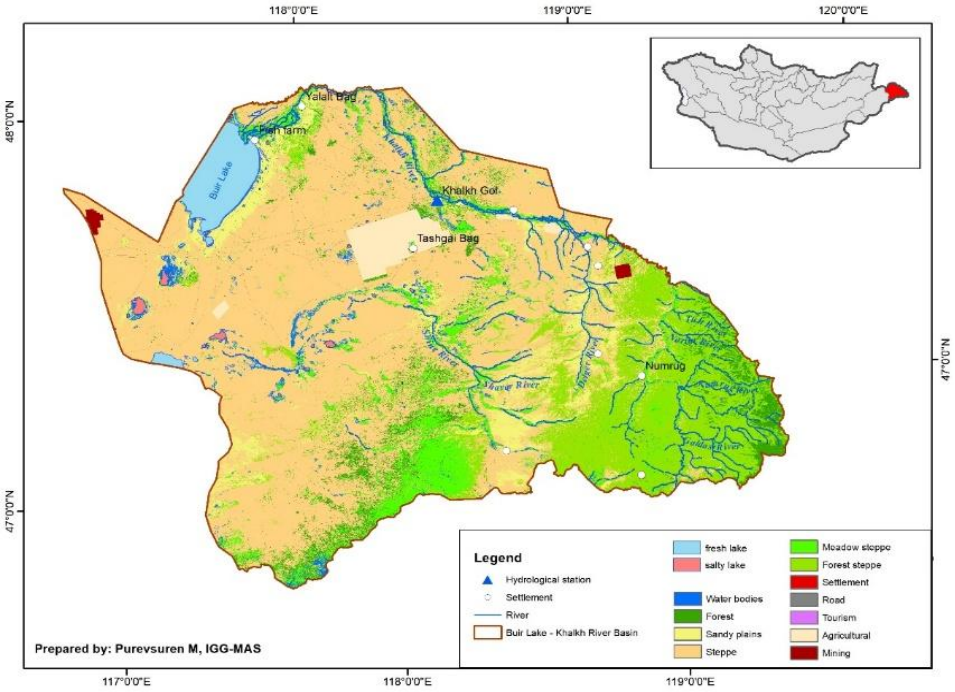

Figure 11. Land use and land cover map of the study area, 2022.

Table 4 highlights key hydrological dynamics across various LULC classes in the Buir Lake-Khalkh River Basin. The steppe, which has a positive water yield of 64.1 mm, benefits from relatively low evapotranspiration (211.3 mm) compared to its precipitation (275.5 mm). Conversely, the forest steppe experiences a slight water deficit, with a negative water yield of -5.3 mm, as its higher precipitation (384.9 mm) is almost entirely offset by evapotranspiration (390.2 mm).

Table 4. Water balance components corresponding with LULC classes.

№	LULC classes	WA+	Area (km^2)	Area (%)	P (mm)	ET (mm)	WY (mm)
1	Water bodies	ULU	1065.2	4.5	254.6	597.2	-342.0
2	Forest	ULU	1225.8	5.2	329.9	305.4	24.8
3	Sandy plains	ULU	2094.9	8.8	296.7	251.7	44.5
4	Steppe	ULU	13118.4	55.2	275.5	211.3	64.1
5	Meadow steppe	ULU	1844.3	7.8	309.3	331.4	-21.4
6	Forest steppe	ULU	3677.5	15.5	384.9	390.3	-5.3
7	Settlements	MLU	6.5	0.0	273.1	250.3	21.0
8	Roads	MLU	66.8	0.3	262.7	193.6	68.7
9	Tourism	MLU	1.1	0.0	244.4	550.2	-301.0
10	Agricultural area	MWU	520.8	2.2	276.4	249.6	26.6
11	Mining area	MWU	58.7	0.2	286.0	220.0	65.8

Sandy plains demonstrate a balanced hydrological profile, maintaining a positive water yield of 44.5 mm with moderate levels of precipitation (296.7 mm) and evapotranspiration (251.7 mm). In stark contrast, water bodies exhibit a significant negative water yield of -342.0 mm, driven by high evapotranspiration (597.2 mm) far surpassing precipitation (254.6 mm). Agricultural and mining areas contribute positively to the water yield, with 26.6 mm and 65.8 mm respectively, which likely indicates to efficient water management in these zones.

WA+ framework outcomes: Resource base and Evapotranspiration sheets

The LULC map prepared for WA+ framework is shown in Figure 12. We used

Vol. 65 No 01(253) 2025
DOI: https://doi.org/10.5564/pmas.v65i01.4204

the conversion table of Karimi et al, 2013 [12] for changing the land cover, and land use classes into 4 types of land use management classes of WA+. Referenced conversion table provides the classes that form the basis for management options in WA+ based on and use classes with similarity in ecosystem services, provisioning services, human interaction and interventions in the hydrological cycle. Most of the area, accounting for 70.3%, is categorized as utilized land use, while protected land constitutes 27.2% including Dornod Mongol and Nömrög specially protected areas with Tashgai Tavan Lake natural reserve area.

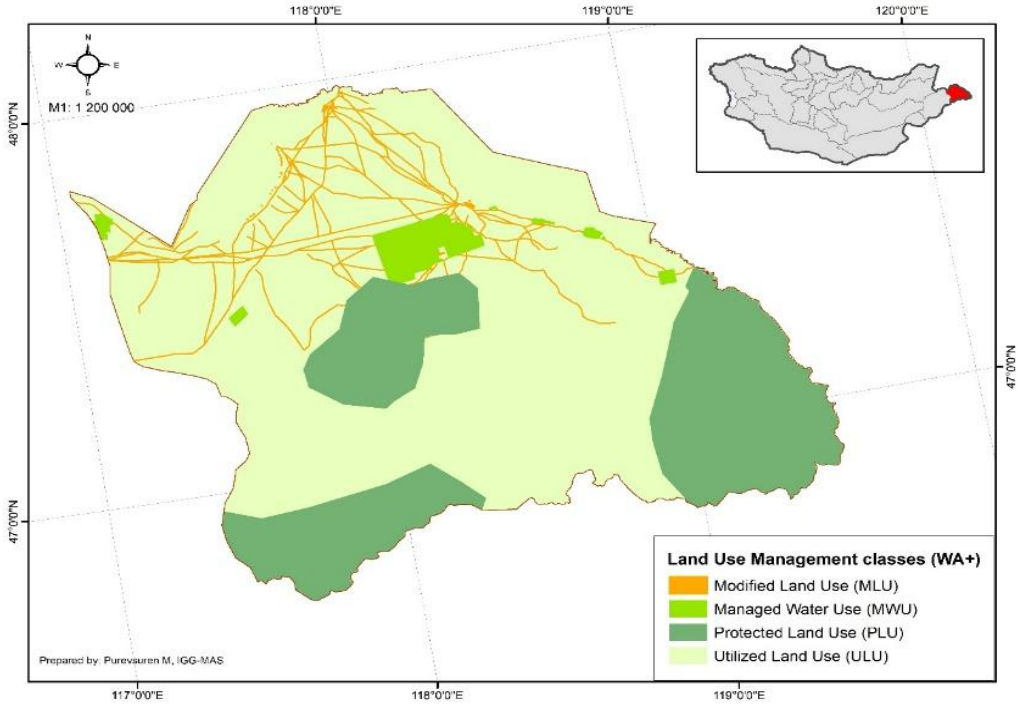

Figure 12. The map of WA+ land use management classes of the study area, 2022.

Sheet 1: Resource base sheet

The WA+ resource base sheets for the Buir Lake-Khalkh River Basin for the years 2018 and 2019 is shown in (Figure 13). Generally, a resource base sheet provides information on water volumes. Inflows are shown on the left of the resource base sheet diagram, the middle part provides information on how and through what processes the water is depleted within a domain, and information on exploitable water and reports on outflows are summarized on the right in (Figure 13).

In 2018, the basin experienced a net inflow of 8.1 km³/year, primarily driven by precipitation and external surface water flows from Khalkh Gol. Out of this, 4.6 km³/year was lost through landscape evapotranspiration, with significant portions attributed to protected and utilized land use areas, which consumed 1.7 km³/year and 2.8 km³/year, respectively. Meanwhile, the exploitable water after evapotranspiration and other consumptive uses amounted to 3.5 km³/year, of which 0.7 km³/year was utilized for human activities, and 2.8 km³/year was reserved as committed environmental outflow, ensuring the sustainability of downstream ecosystems. In 2019, the net inflow decreased slightly to 7.5 km³/year, and 5.4 km³/year was consumed through landscape evapotranspiration. Similar to 2018, the majority of ET occurred over protected land

Vol. 65 No 01(253) 2025
DOI: https://doi.org/10.5564/pmas.v65i01.4204

use (1.8 km³/year) and utilized land use (3.4 km³/year). However, the available exploitable water dropped to 2.1 km³/year, with a minimal portion (0.7 km³/year) utilized for human activities. The utilizable outflow in 2019 was significantly lower at 1.4 km³/year, reflecting a reduction in the water available for downstream environmental commitments and human use.

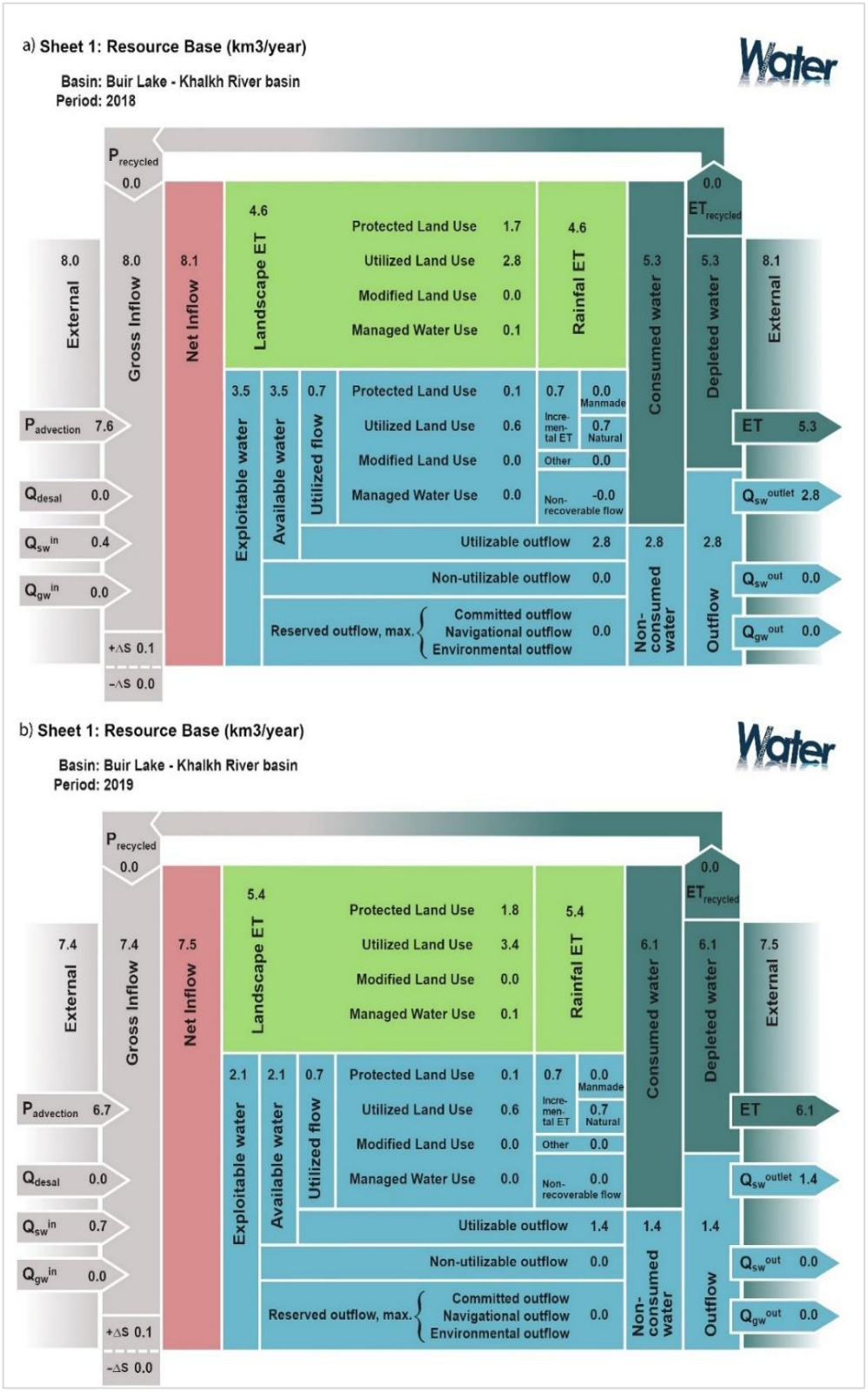

Figure 13. WA+ resource base sheet for the years, a) 2018, and b) 2019.

Vol. 65 No 01(253) 2025
DOI: https://doi.org/10.5564/pmas.v65i01.4204

Sheet 2: Evapotranspiration sheet

Evaporation (E), interception (I) and transpiration (T) data were estimated from the WAPOR V3 dataset of the remote sensing product for generating WA+ evapotranspiration sheet. Values of these

Based on the evapotranspiration results provided in WA+ accounting sheet 2 for the Buir Lake-Khalkh River Basin in three components are then presented per land use type in the center of the sheet. The totals per river basin are visible on the right side while on the left side the total ET is also partitioned into beneficial and non-beneficial (Figure 14).

2018 and 2019, total evapotranspiration (ET) showed a slight decline from 5.4 km³/year in 2018 to 5.3 km³/year in 2019.

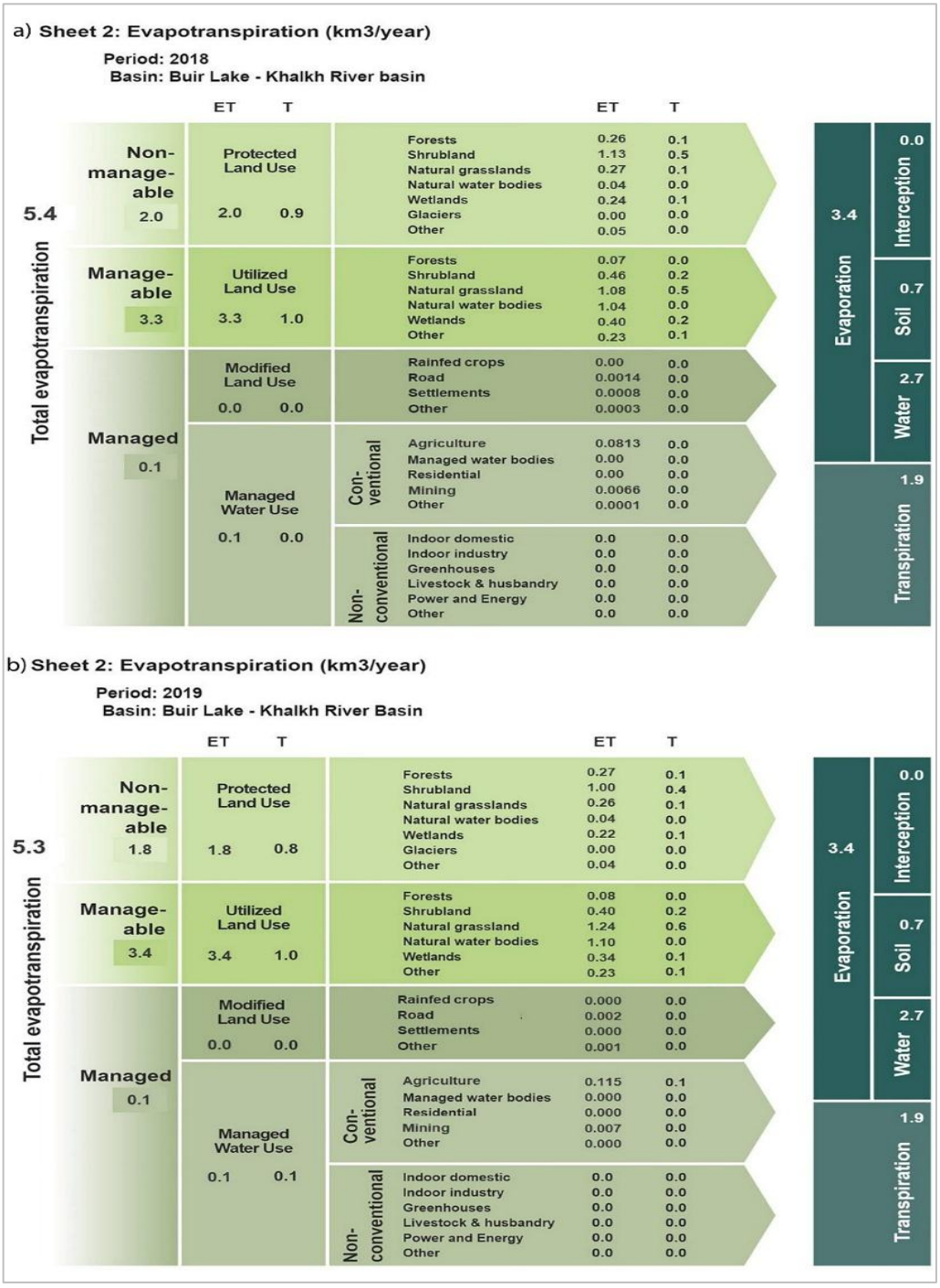

Figure 14. WA+ evapotranspiration sheet for the year a) 2018 and b) 2019.

Vol. 65 No 01(253) 2025
DOI: https://doi.org/10.5564/pmas.v65i01.4204

In the WA+ accounting sheet 2 for the Buir Lake-Khalkh River Basin, the land use/land cover (LULC) classification categorizes steppe as natural grassland, meadow steppe as wetlands, and forest steppe as shrubland. This classification provides a clearer understanding of how each specific LULC type contributes to evapotranspiration (ET) dynamics. The natural grassland (steppe) shows a stable ET contribution of 1.08 km³/year in 2018 and 1.24 km³/year in 2019, highlighting its role as a dominant water consumer within the basin.

The wetlands (meadow steppe) exhibit a slight decrease in ET from 0.42 km³/year in 2018 to 0.34 km³/year in 2019, suggesting potential variability in wetland conditions. The shrubland (forest steppe) ET remains relatively constant, with 1.13 km³/year in 2018 and 1.00 km³/year in 2019, reflecting the consistent water usage by this LULC category.

The non-manageable portion, primarily associated with protected land uses, such as forests, shrubland, and natural grasslands, contributed significantly to total ET, with a small reduction from 2.0 km³/year in 2018 to 1.8 km³/year in 2019. Within the manageable category, utilized land uses, such as forests, shrubland, and natural grasslands accounted for approximately 3.3 km³/year in 2018 and 3.4 km³/year in 2019, suggesting stable water use dynamics in managed areas. Managed water use contributed minimally to overall ET, with values of 0.1 km³/year in both years, while no evapotranspiration was reported for modified land use.

CONCLUSIONS

The study successfully employed the Water Accounting Plus (WA+) framework to assess water resource dynamics in the Buir Lake-Khalkh River Basin, providing some valuable insights into the region's hydrological processes. The analysis demonstrated significant inter-annual and seasonal variability in precipitation (P), evapotranspiration (ET), and water yield (WY) during the period from 2010 to 2021. Precipitation levels fluctuated between 386.3 mm and less than 250 mm, underscoring the region's vulnerability to changes in water availability. Concurrently, evapotranspiration exhibited considerable variability, reflecting its strong seasonal component and sensitivity to climatic conditions. Water yield (WY) was found to be significantly influenced by land use and land cover (LULC) types. Specifically, steppe areas contributed a positive water yield of 64.1 mm, indicating their importance in water generation, while water bodies displayed a substantial water deficit of -342 mm, primarily attributable to elevated evapotranspiration rates. These findings suggest that the region's water balance is shaped by land cover, with natural landscapes like steppes and forests playing key roles in water retention and evapotranspiration dynamics.

The WA+ resource base and evapotranspiration sheets for 2018 and 2019 provided detailed insights into inflows, outflows, and water depletion, highlighting the significance of both protected and utilized land areas in water resource generation. The resource base sheet emphasized the considerable contribution of these land use types to water consumption, while the evapotranspiration sheet elucidated the distribution of evaporation, transpiration, and interception across various LULC types. Steppe areas consistently exhibited high water consumption, with ET values of 1.08 km³/year in 2018 and 1.24 km³/year in 2019, while wetlands demonstrated more variability in water use, reflecting changing hydrological conditions. Overall, the findings derived from the WA+ framework suggest an urgent need for improved water management strategies, particularly in regions characterized by significant evapotranspiration, such as steppes and protected lands. The identification of exploitable water resources and its allocation of these resources between human use and environmental needs, as

Vol. 65 No 01(253) 2025
DOI: https://doi.org/10.5564/pmas.v65i01.4204

outlined in the resource base sheet, is crucial for effective water governance. With evapotranspiration identified as the primary mechanism of water depletion, policies aimed at enhancing water retention and mitigating unnecessary ET are essential for improving overall water availability in the basin.

While this study demonstrates the utility of satellite-based datasets for implementing the WA+ framework in data-scarce environments, it is important to recognize that remote sensing products carry inherent uncertainties. In particular, GRACE-FO data, though valuable for tracking total water storage anomaly (TWSA), is spatially coarse and was originally designed for larger-scale hydrological systems. As such, its application in small to medium-sized basins, like the Buir Lake–Khalkh River Basin, may lead to spatial averaging effects and reduced sensitivity to localized hydrological changes. This limitation introduces uncertainty into the estimation of water storage variations and, consequently, the WA+ water balance outputs. Therefore, future studies should prioritize the integration of ground-based measurements - such as streamflow, groundwater levels, and meteorological station data - to complement satellite observations. This hybrid approach would enhance the reliability of input data, improve model calibration and validation, and lead to more robust and context-specific water resource assessments.

Acknowledgements
The study was conducted as a part of a research project titled “Assessing the Tourism Carrying Capacity of Buir and Khyargas Lake Based on the Estimation of Ecosystem Services Value”. The authors extend their sincere gratitude to the project leader, Dr. Renchinmyadag, for her invaluable insights that significantly contributed to the enhancement of the research outcomes. Additionally, appreciation is expressed to the team of the Authority of Buir Lake-Khalkh River Basin for providing hydrological and meteorological data, which were crucial for the successful execution of this study.

Ethical approval
This study did not involve human participants. Therefore, ethical approval was not required. All data collection and analysis procedures were complied with institutional, national, and international guidelines relevant to environmental research.

Author contributions
P. M., and B. Ts. contributed to the design, idea generating, analysis, conceptualization; P. M. performed WA+ methodology; P. M, B. Ts, and B. B. prepared spatial data for processing, interpreted the results; P. M. wrote original draft preparation; B. Ts, and B. B. contributed to writing results and discussion, and advising. The final manuscript ,before submission, was checked and approved by all the authors.

Source of funding
This research was funded by the Mongolian Foundation for Science and Technology (grant No. 2022/315).

Conflict of interest
The authors declare there is no conflict of interest.

Vol. 65 No 01(253) 2025
DOI: https://doi.org/10.5564/pmas.v65i01.4204

REFERENCES

1. Mitsch, W. J., and Gosselink, J. G. Wetlands, Fifth edition. Hoboken, NJ: John Wiley and Sons, Inc, 2015. ISBN: 978-1118676820.
2. Gleick, P. H. Water, Drought, Climate Change, and Conflict in Syria. Weather, Climate, and Society, vol. 6, no. 3, pp. 331-340, 2014. https://doi.org/10.1175/WCAS-D-13-00059.1.
3. Dalai, S., Dambaravjaa, O., and Pürevjav, G. Water Challenges in Ulaanbaatar, Mongolia. in Urban Drought, B. Ray and R. Shaw, Eds., in Disaster Risk Reduction. Singapore: Springer Singapore, pp. 347-361, 2019. https://doi.org/10.1007/978-981-10-8947-3_20.
4. Banerjee, R., Möller-Gulland, J., van der Linden, W., Khardaeva, O., Retter, M., Subramanian, S., and Eickmann, C. Mongolia: Targeted analysis on water resources management issues. Technical Report. Washington, DC, USA: 2030 Water Resources Group, 2014. https://www.2030wrg.org/mongolia-targeted-analysis-wrm-issues.
5. Tumur, B., Jamsran, U., and Zorigtbaatar, N. Rangeland ecosystems of Mongolia. Ulaanbaatar: Munkhiin Useg LLC, 2018.
6. Ministry of Environment and Green Development. Integrated Water Management Plan of Mongolia. Ulaanbaatar, Mongolia, 2013. ISBN 978-99962-4-555-8.
7. Garmaa, D. Current Situation of Water Resources Management in Mongolia. Magazine of the Korean Society of Agricultural Engineers, vol. 49, no. 2, pp. 43–60, 2007. https://koreascience.kr/article/JAKO200708349650884.pdf.
8. Bogra, S. Water Provisioning Services. in Engineering and Ecosystems, B. R. Bakshi, Ed. Cham: Springer International Publishing, pp. 65–84. 2023. https://doi.org/10.1007/978-3-031-35692-6_4.
9. Siebert, S., Burke, J., Faures, J. M., Frenken, K., Hoogeveen, J., Döll, P., and Portmann, F. T. Groundwater use for irrigation – a global inventory. Hydrology and earth system sciences, vol. 14, no. 10, pp. 1863–1880, 2010. https://doi.org/10.5194/hess-14-1863-2010.
10. Salvadore, E., Mul, M., Tran, B., and Karimi, P. Water Accounting study for three sub-basins of the Krishna water system in Karnataka, India. IHE Delft Institute for Water Education, The Netherlands, Project report, 2020.
11. Molden, D. Accounting for Water Use and Productivity. Colombo, Sri Lanka: International Irrigation Management Institute, 1998. ISBN 929090-349.
12. Karimi, P., Bastiaanssen, W. G. M., and Molden, D. Water Accounting Plus (WA+) - a water accounting procedure for complex river basins based on satellite measurements. Hydrology and Earth System Sciences, vol. 17, no. 7, pp. 2459–2472, 2013. https://doi.org/10.5194/hess-17-2459-2013.
13. Michailovsky, C., Pareeth, S., Karimi, P., and Mul, M. Water Accounting and Productivity for the Selenge River Basin, Mongolia. IHE Delft Institute for Water Education, The Netherlands, Project report, 2020.
14. Mönkhtsetseg, Z., Dorjsüren, D., and Jargaltulga, T. Estimation and application of the water resources distribution using the Water Accounting Plus: A case study of the Kherlen River basin. Geographical Issues, vol. 22, no. 02, pp. 30–43, 2022. https://doi.org/10.22353/.v22i02.1272.
15. Singh, V. G., Singh, S. K., Kumar, N., Kumar, P., Gupta, P. K., Singh, P. K., Gašparović, M., Ray, R. L. and Saito, O. Water Accounting Using Satellite Products and Water Accounting Plus

Vol. 65 No 01(253) 2025
DOI: https://doi.org/10.5564/pmas.v65i01.4204

Framework in a Semi-Arid Betwa River Basin, India. Water, vol. 14, no. 21, p. 3473, 2022. https://doi.org/10.3390/w14213473.
16. Asian Development Bank. Overview of Mongolia's Water Resources System and Management: Country Water Security Assessment. 2020. https://doi.org/10.22617/TCS200202-2.
17. Ramsar Convention Secretariat. Information Sheet on Ramsar Wetlands (RIS) for Lake Buir and its surrounding wetlands. Mar. 19, 2004. Accessed: Apr 17, 2025. [Online]. Available: https://rsis.ramsar.org/RISapp/files/RISrep/MN1377RIS.pdf.
18. Orkhonselenge, A., Uuganzaya, M., and Davaagatan, T. Landscape, Lake Distribution, and Evolution in Eastern Mongolia. in Lakes of Mongolia, in Syntheses in Limnogeology, Cham: Springer International Publishing, pp. 79–102, 2022. https://doi.org/10.1007/978-3-030-99120-3_6.
19. Yembuu, B., Ed. The Physical Geography of Mongolia, in Geography of the Physical Environment, Cham: Springer International Publishing, 2021. https://doi.org/10.1007/978-3-030-61434-8.
20. Zepner, L., Karrasch, P., Wiemann, F., and Bernard, L. ClimateCharts.net - an interactive climate analysis web platform. International Journal of Digital Earth, vol. 14, no. 3, pp. 338–356, 2021. https://doi.org/10.1080/17538947.2020.1829112.
21. Davaa, G., Ed. Surface Water Regime and Resources of Mongolia. Ulaanbaatar: Admon printing LLC, 2015. ISBN: 978-99973-0-767-5.
22. WWF Mongolia, Wetland of International Importance: Buir Lake. 2021. Accessed: Apr 17, 2025. [Online]. Available: https://wwfasia.awsassets.panda.org/downloads /buir_nuur_ramsar.pdf.
23. Tserensodnom, J. Catalog of Mongolian Lakes. Ulaanbaatar: Shuvuun Saaral, 2000.
24. Karimi, P., Bastiaanssen, W. G. M., Molden, D., and Cheema, M. J. M. Basin-wide water accounting based on remote sensing data: an application for the Indus Basin. Hydrology and Earth System Sciences, vol. 17, no. 7, pp. 2473–2486, 2013. https://doi.org/10.5194/hess-17-2473-2013.
25. Falkenmark, M., and Rockström, J. The New Blue and Green Water Paradigm: Breaking New Ground for Water Resources Planning and Management. Journal of Water Resources Planning and Management, vol. 132, no. 3, pp. 129–132, 2006, https://doi.org/10.1061/(ASCE)0733-9496(2006)132:3(129).
26. Hillel, D. Introduction to Environmental Soil Physics. Burlington: Elsevier Science, 2003. ISBN: 978-14933-0-063.
27. Fick, S. E., and Hijmans, R. J. WorldClim 2: new 1-km spatial resolution climate surfaces for global land areas. International Journal of Climatology, vol. 37, no. 12, pp. 4302–4315, 2017. https://doi.org/10.1002/joc.5086.
28. Allen, R. G., Tasumi, M., and Trezza, R. Satellite-Based Energy Balance for Mapping Evapotranspiration with Internalized Calibration (METRIC)-Model. Journal of Irrigation and Drainage Engineering, vol. 133, no. 4, pp. 380–394, 2007. https://doi.org/10.1061/(ASCE)0733-9437(2007)133:4(380).
29. Velpuri, N. M., and Senay, G. B. Partitioning Evapotranspiration into Green and Blue Water Sources in the Conterminous United States. Scientific Reports, vol. 7, no. 1, p. 6191, 2017. https://doi.org/10.1038/s41598-017-06359-w.

Vol. 65 No 01(253) 2025
DOI: https://doi.org/10.5564/pmas.v65i01.4204

30. Lin, C., Wu, C. C., Tsogt, K., Ouyang, Y. C., and Chang, C. I. Effects of atmospheric correction and pansharpening on LULC classification accuracy using WorldView-2 imagery. Information Processing in Agriculture, vol. 2, no. 1, pp. 25–36, 2015. https://doi.org/10.1016/j.inpa.2015.01.003.
31. Karimi, P., and Bastiaanssen, W. G. M. Spatial evapotranspiration, rainfall and land use data in water accounting - Part 1: Review of the accuracy of the remote sensing data. Hydrology and Earth System Sciences, vol. 19, no. 1, pp. 507–532, 2015. https://doi.org/10.5194/hess-19-507-2015.
32. Chen, J., Cazenave, A., Dahle, C., Llovel, W., Panet, I., Pfeffer, J., and Moreira, L. Applications and Challenges of GRACE and GRACE Follow-On Satellite Gravimetry. Surveys in Geophysics, vol. 43, no. 1, pp. 305–345, 2022. https://doi.org/10.1007/s10712-021-09685-x.